

Supporting Information for
Spin-State Energetics and Magnetic Anisotropy in
Penta-coordinated Fe(III) Complexes with Different Axial and
Equatorial Ligand Environments

Shalini Joshi, Sabyasachi Roy Chowdhury, and Sabyashachi Mishra*

Department of Chemistry, Indian Institute of Technology Kharagpur, Kharagpur, India

* mishra@chem.iitkgp.ac.in

TABLE S1: The optimized energy (in cm^{-1}) of the complex $\text{Fe}_{\text{Cl}}^{\text{P}}$ in different spin-states with different functionals (M052X functional gives one imaginary frequency for the non-planar conformer of complex $\text{Fe}_{\text{Cl}}^{\text{P}}$ in the IS state). The energy of the intermediate-spin state with planar conformation of the phenyl rings is taken as reference.

Functionals	Intermediate-Spin State		High-Spin State	
	Planar	Non-Planar	Planar	Non-Planar
CAM-B3LYP	0.0	-447.3	594.8	786.4
B3LYP	0.0	-44.2	920.3	1095.3
PBE	0.0	-156.9	3488.9	3420.1
BLYP	0.0	102.7	3150.5	3394.6
M06L	0.0	-522.2	-1631.0	-1845.4
M05	0.0	-437.9	-2979.8	-3102.2
M052X	0.0	-468.6	-2691.6	-2657.9

TABLE S2: The comparison of the geometrical parameters and RMSD (with respect to the X-ray structure) of the complex $\text{Fe}_{\text{Cl}}^{\text{P}}(\text{np.})$ optimized in its intermediate-spin state with CAM-B3LYP, B3LYP, PBE functionals.

Functional	Fe-equatorial (\AA)	Fe-axial (\AA)	$\angle \text{A-Fe-A}$ ($^\circ$)	$\angle \text{E-Fe-E}$ ($^\circ$)	RMSD (\AA)
CAM-B3LYP	2.30, 2.26, 2.23	2.33	177.4	129.3, 117.7, 112.9	0.053
B3LYP	2.32, 2.28, 2.25	2.35	177.1	129.7, 118.1, 112.3	0.061
PBE	2.29, 2.25, 2.22	2.32	176.1	129.7, 118.8, 111.5	0.066
Experiment	2.30, 2.25, 2.23	2.36	175.1	125.4, 117.5, 117.1	

TABLE S3: Energy of d-orbitals (in cm^{-1}) of the modeled complexes. The energy of the d_{xz} orbital is taken as reference.

Complex	Planar					Non-planar				
	d_{xz}	d_{yz}	d_{xy}	$d_{x^2-y^2}$	d_{z^2}	d_{xz}	d_{yz}	d_{xy}	$d_{x^2-y^2}$	d_{z^2}
Fe_{Cl}^P	0	198	5223	5399	22299	0	614	5048	6057	22738
Fe_F^P	0	2963	8164	10535	21816	0	2985	8164	10557	21860
Fe_{Br}^P	0	593	4060	4587	23067	0	351	4082	4697	23022
Fe_I^P	0	527	2721	3292	23396	0	329	2875	3885	24493
Fe_{Cl}^N	0	922	1317	2348	9503	0	198	3665	4587	10973
Fe_{Cl}^{As}	0	505	5333	5750	20982	0	680	5070	6145	20894
Fe_{Br}^{As}	0	461	4214	4609	21706	0	373	4170	4806.5	21684
Fe_I^{As}	0	373	2941	3358	22628	0	154	3051	3424	22584
Fe_{Cl}^{N,P}	0	987	3687	4324	17075	0	439	4280	5114	18063
Fe_{Cl}^{P,ac.}	0	329	5026	5531	21706	0	988	6409	4872	22079
Fe_{Br}^{P,ac.}	0	198	3841	4236	22035	0	724	3841	5092	22364
Fe_I^{P,ac.}	0	1273	4258	1449	12642	0	461	3599	2546	22628
Fe_{Cl}^{As,ac.}	0	483	5245	5684	20214	0	483	5245	5684	20214
Fe_{Br}^{As,ac.}	0	285	4411	4104	20816	0	285	4126	4411	20916
Fe_I^{As,ac.}	0	241	2831	3073	21904	0	373	3665	2875	21991

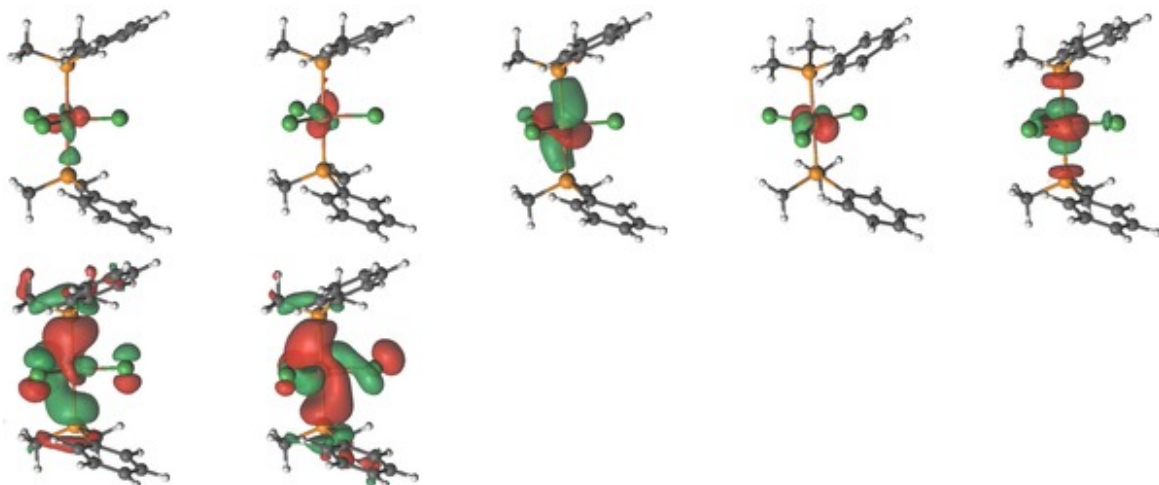


FIG. S1: The active-space (canonical) orbitals from (9,7) SA-CASSCF calculation for $\text{Fe}_{\text{Cl}}^{\text{P}}(\text{np.})$ complex. The five orbitals in the upper row are (predominantly) metal d-orbitals, while the two orbitals in the lower row are ligand orbitals.

TABLE S4: DFT optimized geometrical parameters (distance in Å and angle in °) of Fe(III) complexes in the intermediate spin states. Here, $\delta = \sum_{i=1}^3 |120 - \alpha_i|$ with α_i representing the three equatorial angles.

Complex	Intermediate-Spin State				High-Spin State		
	Fe-equatorial	Fe-axial	\angle A-Fe-A	δ	Fe-equatorial	Fe-axial	\angle A-Fe-A
$\text{Fe}_{\text{Cl}}^{\text{P}}(\text{pl.})$	2.26, 2.26, 2.24	2.33	178.6	4	2.26, 2.23, 2.23	2.55	172.9
$\text{Fe}_{\text{Cl}}^{\text{P}}(\text{np.})$	2.30, 2.26, 2.23	2.33	177.4	18	2.26, 2.23, 2.23	2.55	174.2
$\text{Fe}_{\text{F}}^{\text{P}}(\text{pl.})$	1.93, 1.82, 1.79	2.31	169.5	52	1.83, 1.82, 1.81	2.56	169.0
$\text{Fe}_{\text{F}}^{\text{P}}(\text{np.})$	1.93, 1.82, 1.79	2.31	169.5	52	1.83, 1.82, 1.81	2.56	169.0
$\text{Fe}_{\text{Br}}^{\text{P}}(\text{pl.})$	2.44, 2.39, 2.39	2.34	177.3	15	2.41, 2.39, 2.39	2.55	175.7
$\text{Fe}_{\text{Br}}^{\text{P}}(\text{np.})$	2.44, 2.39, 2.39	2.34	178.8	14	2.41, 2.40, 2.39	2.54	177.1
$\text{Fe}_{\text{I}}^{\text{P}}(\text{pl.})$	2.61, 2.61, 2.65	2.36	178.5	16	2.61, 2.61, 2.61	2.56	178.7
$\text{Fe}_{\text{I}}^{\text{P}}(\text{np.})$	2.58, 2.58, 2.58	2.35	179.6	21	2.62, 2.61, 2.61	2.55	179.0
$\text{Fe}_{\text{Cl}}^{\text{N}}(\text{pl.})$	2.30, 2.23, 2.23	2.15	179.4	23	2.21, 2.21, 2.20	2.39	176.5
$\text{Fe}_{\text{Cl}}^{\text{N}}(\text{np.})$	2.26, 2.26, 2.24	2.17	178.1	16	2.21, 2.19, 2.19	2.38	179.5
$\text{Fe}_{\text{Cl}}^{\text{As}}(\text{pl.})$	2.29, 2.24, 2.24	2.41	175.2	11	2.25, 2.22, 2.22	2.65	173.5
$\text{Fe}_{\text{Cl}}^{\text{As}}(\text{np.})$	2.29, 2.26, 2.22	2.41	175.9	20	2.25, 2.22, 2.22	2.65	173.4
$\text{Fe}_{\text{Br}}^{\text{As}}(\text{pl.})$	2.44, 2.39, 2.39	2.41	176.3	12	2.41, 2.38, 2.38	2.64	174.2
$\text{Fe}_{\text{Br}}^{\text{As}}(\text{np.})$	2.44, 2.40, 2.39	2.41	177.9	14	2.40, 2.38, 2.38	2.64	175.1
$\text{Fe}_{\text{I}}^{\text{As}}(\text{pl.})$	2.65, 2.61, 2.61	2.43	177.4	13	2.61, 2.59, 2.59	2.64	176.5
$\text{Fe}_{\text{I}}^{\text{As}}(\text{np.})$	2.65, 2.65, 2.61	2.43	178.5	10	2.61, 2.60, 2.60	2.63	179.0
$\text{Fe}_{\text{Cl}}^{\text{N,P}}(\text{pl.})$	2.29, 2.24, 2.24	2.31, 2.18	178.7	18	2.23, 2.22, 2.22	2.54, 2.38	179.6
$\text{Fe}_{\text{Cl}}^{\text{N,P}}(\text{np.})$	2.29, 2.24, 2.24	2.30, 2.17	179.2	16	2.23, 2.22, 2.22	2.53, 2.37	178.4
$\text{Fe}_{\text{Cl}}^{\text{P,ac.}}(\text{pl.})$	2.28, 2.24, 2.23	2.33	171.6	10	2.25, 2.23, 2.21	2.57	168.7
$\text{Fe}_{\text{Cl}}^{\text{P,ac.}}(\text{np.})$	2.30, 2.24, 2.22	2.33	175.6	32	2.25, 2.23, 2.20	2.58	172.7
$\text{Fe}_{\text{Br}}^{\text{P,ac.}}(\text{pl.})$	2.43, 2.39, 2.39	2.34	171.2	8	2.41, 2.39, 2.36	2.56	167.5
$\text{Fe}_{\text{Br}}^{\text{P,ac.}}(\text{np.})$	2.45, 2.40, 2.38	2.35	175.0	29	2.40, 2.39, 2.35	2.58	172.7
$\text{Fe}_{\text{I}}^{\text{P,ac.}}(\text{pl.})$	2.66, 2.61, 2.59	2.37	174.5	29	2.62, 2.61, 2.57	2.58	169.9
$\text{Fe}_{\text{I}}^{\text{P,ac.}}(\text{np.})$	2.67, 2.61, 2.59	2.37	174.2	40	2.60, 2.60, 2.56	2.60	172.5
$\text{Fe}_{\text{Cl}}^{\text{As,ac.}}(\text{pl.})$	2.29, 2.26, 2.22	2.42	174.5	10	2.20, 2.26, 2.26	2.35	174.1
$\text{Fe}_{\text{Cl}}^{\text{As,ac.}}(\text{pl.})$	2.29, 2.26, 2.22	2.42	174.5	10	2.22, 2.25, 2.31	2.33	171.4
$\text{Fe}_{\text{Br}}^{\text{As,ac.}}(\text{pl.})$	2.44, 2.40, 2.38	2.42	173.6	8	2.41, 2.37, 2.37	2.65	171.7
$\text{Fe}_{\text{Br}}^{\text{As,ac.}}(\text{pl.})$	2.44, 2.40, 2.38	2.42	173.6	8	2.40, 2.38, 2.35	2.67	174.3
$\text{Fe}_{\text{I}}^{\text{As,ac.}}(\text{pl.})$	2.65, 2.61, 2.60	2.43	172.4	7	2.62, 2.59, 2.57	2.66	170.2
$\text{Fe}_{\text{I}}^{\text{As,ac.}}(\text{np.})$	2.66, 2.62, 2.59	2.44	176.2	22	2.61, 2.59, 2.56	2.67	174.6

TABLE S5: The configuration state functions (CSF) of the Ground state and lower excited states of the non-planar conformer of all complexes with CSF weight > 5% from a CAS(9,7) calculation. The first two (of the 7 active) orbitals are of ligand type and the next five are of metal d-orbitals. The ground, first, second, and third excited states have dominant electronic configurations $d_{xz}^2 d_{yz}^1 d_{xy}^1 d_{x^2-y^2}^1 d_{z^2}^0$, $d_{xz}^1 d_{yz}^2 d_{xy}^1 d_{x^2-y^2}^1 d_{z^2}^0$, $d_{xz}^1 d_{yz}^1 d_{xy}^2 d_{x^2-y^2}^0 d_{z^2}^0$, and $d_{xz}^1 d_{yz}^1 d_{xy}^1 d_{x^2-y^2}^2 d_{z^2}^0$, respectively. The occupancy of the orbitals is given by 2, u/d (1 electron), and 0.

Complex	Ground state weight(%)	Ist excited state weight(%)
Fe^P_{Cl}	222uuu0	78.2
	u22duuu	8.7
	022uuu2	5.3
Fe^P_{Br}	222uuu0	79.1
	u22duuu	8.1
	022uuu2	6.1
Fe^P_I	222uuu0	80.5
	u22duuu	6.9
	022uuu2	6.7
Fe^{As}_{Br}	222uuu0	77.7
	u22duuu	8.6
	022uuu2	6.8
Fe^{As}_I	222uuu0	78.7
	u22duuu	7.5
	022uuu2	7.7
Fe^{P,ac.}_{Cl}	222uuu0	76.4
	u22duuu	9.5
	022uuu2	5.5
Fe^{P,ac.}_{Br}	222uuu0	77.6
	u22duuu	8.7
	022uuu2	6.4
Fe^{P,ac.}_I	222uuu0	78.1
	u22duuu	8.1
	022uuu2	7.3
Fe^{As,ac.}_I	222uuu0	77.6
	u22duuu	7.9
	022uuu2	8.0

TABLE S6: Same as in Table S5 for the planar conformers of the complexes.

Complex	Ground state weight(%)	Ist excited state weight(%)
Fe^P_{Cl}	222uuu0	78.9
	u22duuu	8.7
	022uuu2	5.1
Fe^P_{Br}	222uuu0	78.9
	u22duuu	8.3
	022uuu2	5.9
Fe^P_I	222uuu0	78.6
	u22duuu	7.9
	022uuu2	6.9
Fe^{As}_{Br}	222uuu0	77.8
	u22duuu	8.7
	022uuu2	6.5
Fe^{As}_I	222uuu0	78.4
	u22duuu	7.8
	022uuu2	7.5
Fe^{P,ac.}_{Cl}	222uuu0	77.8
	u22duuu	9.1
	022uuu2	5.2
Fe^{P,ac.}_{Br}	222uuu0	73.9
	u22duuu	8.2
	022uuu2	5.7
Fe^{P,ac.}_I	222uu0u	22.6
	u22duuu	43.9
	u22udu	13.0
	022uu2u	9.0
	-	-
		02uu22u
Fe^{As,ac.}_{Cl}	222uuu0	76.1
	u22duuu	10.1
	022uuu2	5.9
Fe^{As,ac.}_{Br}	222uuu0	76.7
	u22duuu	9.1
	022uuu2	6.7
Fe^{As,ac.}_I	222uuu0	55.5
	22u2uu0	22.3
	u22duuu	5.7
	022uuu2	5.5

TABLE S7: Composition of the spin-orbit coupled states (or Kramer's doublets) of planar conformers in terms of the scalar-relativistic states.

Complex	KD1/KD2	KD3/KD4
Fe_{Cl}^P	$0.76 Q_0\rangle+0.23 Q_1\rangle$	$0.93 Q_0\rangle+0.05 Q_1\rangle$
Fe_F^P		
Fe_{Br}^P	$0.92 Q_0\rangle+0.07 Q_1\rangle$	$0.98 Q_0\rangle+0.01 Q_1\rangle$
Fe_I^P	$0.90 Q_0\rangle+0.08 Q_1\rangle+0.01 Q_2\rangle$	$0.97 Q_0\rangle+0.01 Q_1\rangle+0.01 Q_2\rangle$
Fe_{Cl}^N		
Fe_{As}_{Cl}^N		
Fe_{Br}^{As}	$0.89 Q_0\rangle+0.10 Q_1\rangle$	$0.98 Q_0\rangle+0.02 Q_1\rangle$
Fe_I^{As}	$0.87 Q_0\rangle+0.12 Q_1\rangle$	$0.97 Q_0\rangle+0.02 Q_1\rangle$
Fe_{Cl}^{N,P}		
Fe_{Cl}^{P,ac.}	$0.84 Q_0\rangle+0.16 Q_1\rangle$	$0.97 Q_0\rangle+0.03 Q_1\rangle$
Fe_{Br}^{P,ac.}	$0.77 Q_0\rangle+0.22 Q_1\rangle$	$0.94 Q_0\rangle+0.05 Q_1\rangle$
Fe_I^{P,ac.}	$0.97 S_{12}\rangle+0.02 S_{13}\rangle+0.004 Q_1\rangle$	$0.98 S_{12}\rangle+0.01 S_{13}\rangle+0.003 S_{14}\rangle+0.003 Q_1\rangle$
Fe_{Cl}^{As,ac.}	$0.90 Q_0\rangle+0.10 Q_1\rangle$	$0.98 Q_0\rangle+0.02 Q_1\rangle$
Fe_{Br}^{As,ac.}	$0.85 Q_0\rangle+0.14 Q_1\rangle$	$0.97 Q_0\rangle+0.02 Q_1\rangle$
Fe_I^{As,ac.}	$0.79 Q_0\rangle+0.20 Q_1\rangle+0.01 Q_2\rangle$	$0.94 Q_0\rangle+0.04 Q_1\rangle+0.01 Q_2\rangle$

TABLE S8: Composition of the spin-orbit coupled states (or Kramer's doublets) of non-planar conformers in terms of the scalar-relativistic states.

Complex	KD1/KD2	KD3/KD4
Fe_{Cl}^P	$0.91 Q_0\rangle+0.08 Q_1\rangle$	$0.98 Q_0\rangle+0.01 Q_1\rangle$
Fe_F^P		
Fe_{Br}^P	$0.83 Q_0\rangle+0.15 Q_1\rangle$	$0.96 Q_0\rangle+0.02 Q_1\rangle$
Fe_I^P	$0.80 Q_0\rangle+0.18 Q_1\rangle+0.01 Q_2\rangle$	$0.94 Q_0\rangle+0.03 Q_1\rangle+0.01 Q_2\rangle$
Fe_{Cl}^N		
Fe_{As}_{Cl}^N		
Fe_{Br}^{As}	$0.85 Q_0\rangle+0.14 Q_1\rangle$	$0.96 Q_0\rangle+0.02 Q_1\rangle$
Fe_I^{As}	$0.76 Q_0\rangle+0.23 Q_1\rangle$	$0.93 Q_0\rangle+0.06 Q_1\rangle$
Fe_{Cl}^{N,P}		
Fe_{Cl}^{P,ac.}	$0.96 Q_0\rangle+0.04 Q_1\rangle$	$0.99 Q_0\rangle+0.01 Q_1\rangle$
Fe_{Br}^{P,ac.}	$0.93 Q_0\rangle+0.06 Q_1\rangle$	$0.98 Q_0\rangle+0.01 Q_1\rangle$
Fe_I^{P,ac.}	$0.91 Q_0\rangle+0.08 Q_1\rangle+0.01 Q_3\rangle$	$0.97 Q_0\rangle+0.01 Q_1\rangle+0.01 Q_3\rangle$
Fe_{Cl}^{As,ac.}	$0.90 Q_0\rangle+0.10 Q_1\rangle$	$0.98 Q_0\rangle+0.02 Q_1\rangle$
Fe_{Br}^{As,ac.}	$0.85 Q_0\rangle+0.14 Q_1\rangle$	$0.97 Q_0\rangle+0.03 Q_1\rangle$
Fe_I^{As,ac.}	$0.88 Q_0\rangle+0.10 Q_1\rangle+0.01 Q_2\rangle$	$0.97 Q_0\rangle+0.02 Q_1\rangle+0.01 Q_2\rangle+0.01 Q_3\rangle$

TABLE S9: The computed g -tensors for the lowest pair of Kramer's doublet of complexes in the intermediate spin state. The angle (in $^{\circ}$) represents the deviation of the magnetization axis of excited spin-orbit states from the principal anisotropic axis. For complexes $\mathbf{Fe}_{\text{Cl}}^{\text{As,ac.}}$ and $\mathbf{Fe}_{\text{Br}}^{\text{As,ac.}}$, only planar conformation exists.

Planar						Non-planar				
Complex	Energy	g_x	g_y	g_z	angle	Energy	g_x	g_y	g_z	angle
$\mathbf{Fe}_{\text{Cl}}^{\text{P}}$	0	0.02	0.02	7.59		0	0.20	0.20	7.05	
	78	3.69	3.65	2.87	0	41	4.24	3.88	2.41	0
$\mathbf{Fe}_{\text{Br}}^{\text{P}}$	0	0.06	0.06	7.0		0	0.12	0.12	7.39	
	35	4.18	4.05	2.38	0	58	4.08	3.85	2.64	0
$\mathbf{Fe}_{\text{I}}^{\text{P}}$	0	0.50	0.53	7.01		0	0.82	0.93	7.30	
	32	4.67	3.68	2.36	0	59	2.56	3.14	4.69	31
$\mathbf{Fe}_{\text{Br}}^{\text{As}}$	0	0.01	0.01	7.18		0	0.13	0.14	7.32	
	45	4.06	4.06	2.48	0	55	4.12	3.87	2.59	0
$\mathbf{Fe}_{\text{I}}^{\text{As}}$	0	0.18	0.19	7.21		0	0.18	0.18	7.59	
	42	4.30	3.94	2.51	0	69	3.96	3.64	2.87	0
$\mathbf{Fe}_{\text{Cl}}^{\text{P,ac.}}$	0	0.15	0.16	7.37		0	0.15	0.16	6.74	
	60	4.04	3.79	2.61	0	24	4.28	3.97	2.26	0
$\mathbf{Fe}_{\text{Br}}^{\text{P,ac.}}$	0	0.22	0.23	7.55		0	0.45	0.48	6.85	
	72	3.93	3.57	2.82	0	29	4.58	3.68	2.29	0
$\mathbf{Fe}_{\text{I}}^{\text{P,ac.}}$	0	0.01	0.01	10.41		0	1.33	1.72	6.59	
	5	1.23	1.28	6.14	0	32	1.97	2.57	5.47	60
$\mathbf{Fe}_{\text{Cl}}^{\text{As,ac.}}$	0	0.18	0.19	7.15						
	47	4.17	3.87	2.46						
$\mathbf{Fe}_{\text{Br}}^{\text{As,ac.}}$	0	0.20	0.20	7.32						
	55	4.15	3.82	2.58	0					
$\mathbf{Fe}_{\text{I}}^{\text{As,ac.}}$	0	0.37	0.40	7.47		0	0.73	0.82	7.05	
	63	4.23	3.56	2.74	0	39	2.37	3.38	4.85	31

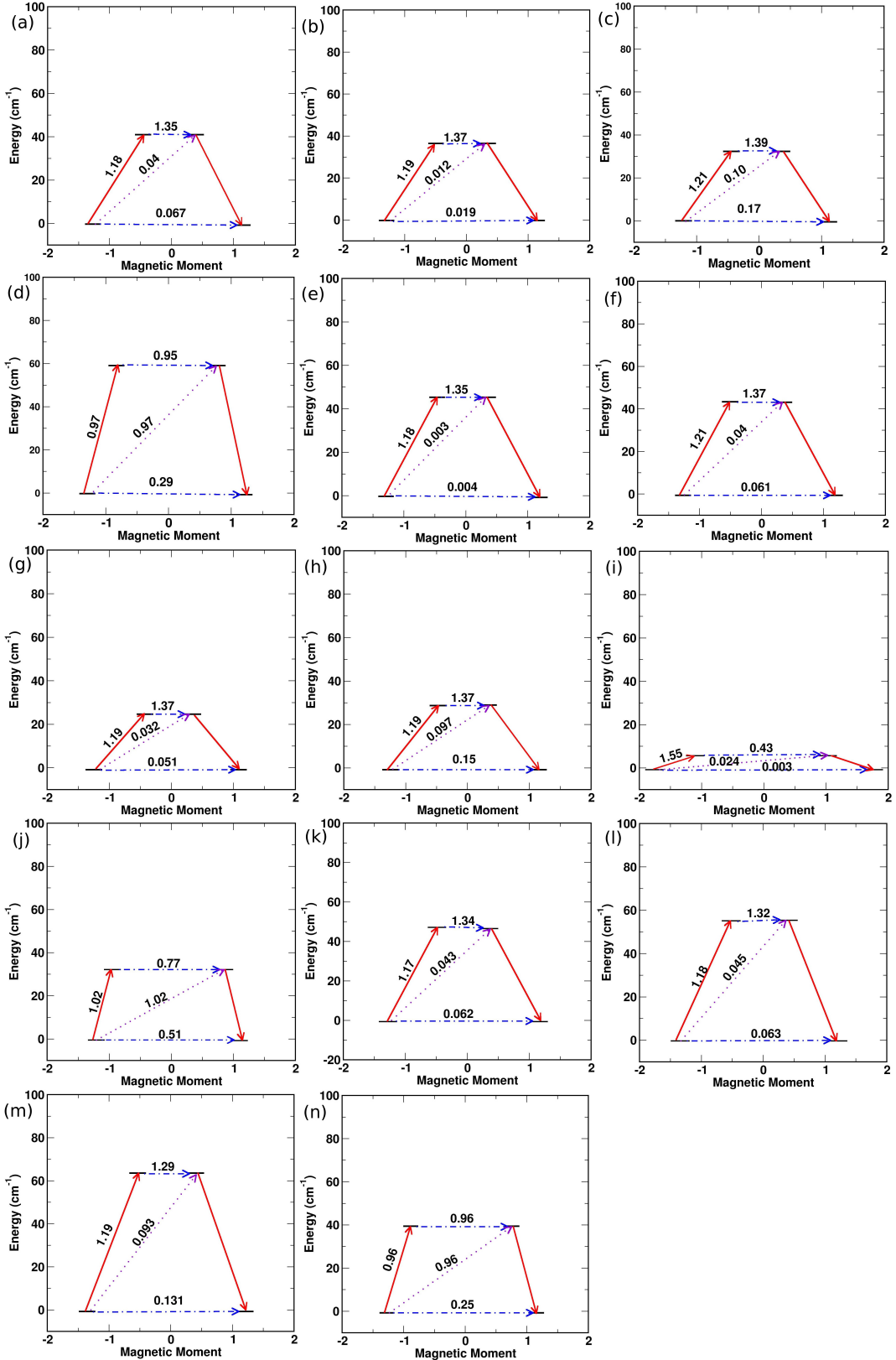


FIG. S2: The mechanism of relaxation of magnetization in the complexes (a) $\text{Fe}_{\text{Cl}}^{\text{P}}(\text{np.})$, (b) $\text{Fe}_{\text{Br}}^{\text{P}}(\text{pl.})$, (c) $\text{Fe}_{\text{I}}^{\text{P}}(\text{pl.})$, (d) $\text{Fe}_{\text{I}}^{\text{P}}(\text{np.})$, (e) $\text{Fe}_{\text{Br}}^{\text{P}}(\text{pl.})$, (f) $\text{Fe}_{\text{I}}^{\text{As}}(\text{pl.})$, (g) $\text{Fe}_{\text{Cl}}^{\text{P},\text{ac.}}(\text{np.})$, (h) $\text{Fe}_{\text{Br}}^{\text{P},\text{ac.}}(\text{np.})$, (i) $\text{Fe}_{\text{I}}^{\text{P},\text{ac.}}(\text{pl.})$, (j) $\text{Fe}_{\text{I}}^{\text{P},\text{ac.}}(\text{np.})$, (k) $\text{Fe}_{\text{Cl}}^{\text{As},\text{ac.}}(\text{pl.})$, (l) $\text{Fe}_{\text{Br}}^{\text{As},\text{ac.}}(\text{pl.})$, (m) $\text{Fe}_{\text{I}}^{\text{As},\text{ac.}}(\text{pl.})$, (n) $\text{Fe}_{\text{I}}^{\text{As},\text{ac.}}(\text{np.})$.

Effect of the number of roots in CASSCF calculation on U_{eff}

To explore the effect of the number of IS and HS excited states on the electronic and magnetic properties of complexes, the SA-CASSCF calculation was performed with the different numbers of roots based on their relative energy separation (Table S11). It is seen that the energy gap between the spin-free states varies with the number of roots. For example, in the case of complex $\text{Fe}_{\text{Cl}}^{\text{P}}(\text{np.})$, by taking all the possible quartet and sextet roots, the first quartet spin-free state lies 550.5 cm^{-1} above the ground state. On the other hand, with a less number of roots, such as 15Q, 10S, and 4Q roots, the energy separation between the ground and first excited spin-free state is 342 cm^{-1} , and 365 cm^{-1} , respectively. The smaller energy gap between the lowest-lying spin-free states gives rise to better mixing of states, resulting in higher splitting between the spin-orbit states. This is the reason for the higher value of magnetic anisotropic parameters (D and U_{eff}) by taking a lesser number of roots (Table S12). It is seen in the case of $\text{Fe}_{\text{Cl}}^{\text{P}}(\text{np.})$, the maximum number of quartet and sextet roots reproduces the experimental U_{eff} value. Thus, all the electronic and magnetic properties of all the designed complexes are analysed by taking all quartet and sextet roots.

TABLE S10: The lowest spin-free and spin-orbit energy levels (in cm^{-1}) of the more stable planar and non-planar conformers of the Fe(III) complexes in the intermediate spin state with the different numbers of roots.

Complex	Spin-free states			Spin-orbit states		
	224(Q), 21(S)	4(Q)	15(Q), 10(S)	224(Q), 21(S)	4(Q)	15(Q), 10 (S)
Fe^P_{Cl}(np.)	550.5	365.7	342.0	40.6	73.2	80.0
	3504.7	5065.6	5668.8	605.1	467.0	451.5
	4400.4	5919.1	6448.3	662.9	553.5	543.1
Fe^P_{Br}(np.)	346.3	224.9	234.0	58.0	95.0	93.2
	2612.7	3975.4	4578.0	425.8	361.3	365.9
	3145.0	4493.4	5078.7	508.2	473.4	474.3
Fe^{As}_{Br}(pl.)	474.8	389.6	354.4	45.1	68.9	74.5
	2891.5	4144.6	4660.3	535.1	484.2	456.0
	3228.7	4440.0	4935.5	603.6	570.1	546.1
Fe^{As}_I(np.)	240.6	146.1	143.8	69.2	107.7	50.7
	1787.4	2744.9	2554.5	339.9	311.5	266.1
	2112.3	3063.6	2946.3	447.8	443.6	423.1
Fe^{P,ac.}_{Cl}(pl.)	349.4	288.4	203.5	60.3	85.4	109.2
	3696.1	5424.5	6724.6	430.9	406.1	357.7
	4172.1	5862.3	8333.8	507.6	504.3	474.0
Fe^{P,ac.}_{Br}(pl.)	248.4	227.6	209.1	72.3	95.1	91.2
	2676.7	4167.5	4497.3	349.6	361.9	336.3
	3030.1	4471.1	4983.1	445.9	473.7	448.3
Fe^{As,ac.}_{Cl}(pl.)	486.5	376.0	349.5	46.8	71.9	79.4
	3924.5	5314.9	5804.4	549.1	474.4	455.9
	4366.3	5768.6	6230.8	611.9	559.3	546.3
Fe^{As,ac.}_{Br}(pl.)	377.6	307.8	212.9	55.0	80.6	96.2
	2909.4	4114.6	4599.3	452.3	419.5	350.5
	3211.4	4410.6	4724.9	530.3	517.0	464.4
Fe^{As,ac.}_I(pl.)	281.4	232.0	2194.7	62.5	91.4	82.1
	1830.3	2825.7	5157.9	368.2	362.5	2211.3
	2059.5	3025.8	6645.7	469.8	478.3	2322.2

TABLE S11: The magnetic-anisotropic parameters (U_{eff} D , E) in cm^{-1} with different numbers of the quartet (Q) and sextet (S) states. A smaller number of states in the state-averaged calculations tend to overestimate the effective anisotropy barrier. The experimental value of the effective anisotropy barrier for $\mathbf{Fe}_{\text{Cl}}^{\text{P}}(\text{np.})$ is 46 cm^{-1} .

Complex	224(Q), 21(S)			4(Q)			15(Q), 10(S)		
	U_{eff}	D	E	U_{eff}	D	E	U_{eff}	D	E
$\mathbf{Fe}_{\text{Cl}}^{\text{P}}(\text{np.})$	41	-20	0.66	73	-37	0.47	81	-40	0.35
$\mathbf{Fe}_{\text{Br}}^{\text{P}}(\text{np.})$	58	-29	-0.54	95	-48	-0.27	93	-47	-0.14
$\mathbf{Fe}_{\text{Br}}^{\text{As}}(\text{pl.})$	45	-23	0.06	69	-35	0.14	75	-37	0.24
$\mathbf{Fe}_{\text{I}}^{\text{As}}(\text{np.})$	69	-34.6	-0.95	108	-54	-0.56	51	-25	3.68
$\mathbf{Fe}_{\text{Cl}}^{\text{P,ac.}}(\text{pl.})$	60	-30	0.76	86	-43	0.48	109	-55	-0.41
$\mathbf{Fe}_{\text{Br}}^{\text{P,ac.}}(\text{pl.})$	72	-36.1	1.34	95	-48	0.62	91	-46	1.40
$\mathbf{Fe}_{\text{Cl}}^{\text{As,ac.}}(\text{pl.})$	47	-23	0.71	72	-36	0.53	79	-40	0.37
$\mathbf{Fe}_{\text{Br}}^{\text{As,ac.}}(\text{pl.})$	55	-27	0.90	81	-40	0.53	96	-48	0.30
$\mathbf{Fe}_{\text{I}}^{\text{As,ac.}}(\text{pl.})$	63	-31	1.96	91	-46	0.77	82	31	-15.88

Double *d*-shell effect

For first-row transition metal complexes, the inclusion of a second set of *d* orbitals is considered to be important in recovering the electron correlation and estimation of that can determine the accuracy of electronic excitation energies from respective orbitals, commonly known as the double *d*-shell effect. To investigate the impact of the double *d*-shell on the magnetic anisotropy parameters, we expanded our active space from (9,7) to (9,12) by accommodating the five 4*d* orbitals of the metal ion. The (9,7) active space can give rise to 224 quartets, which can be subjected to SA-CASSCF calculation. However, for the (9,12) active space, the number of possible configuration state functions being significantly large (151008), they can not be included in the state-average calculations, as per the latest implementation. Hence, we considered the (a) two and (b) four low-lying quartet states of the non-planar $\text{Fe}_{\text{Cl}}^{\text{P}}$ for SA-CASSCF calculation with the (9,12) active space and for consistency, we computed the same with (9,7) active space as well (i.e., 2Q-SA-(9,7) and 4Q-SA-(9,7)). The corresponding spin-free states, spin-orbit states, D , E and U_{eff} parameters are summarized in Table S12 in ESI. The computed D and U_{eff} by these two active spaces are observed to be similar, which suggests that the nature of the CASSCF wavefunction did not change upon inclusion of the double *d*-shell effect. However, considering a limited number of roots (2Q-SA-(9,7) or 4Q-SA-(9,7)), the D and U_{eff} are overestimated as compared to their experimental values. It is to be noted that the nature of the CASSCF wave function largely depends on the number of states considered for the the state-average calculation, and it has been demonstrated in Table S10 and S11, that such state-truncation error in SA-CASSCF calculation results in a significant impact on the scalar-relativistic states, spin-orbit states, hence on the D and U_{eff} parameters as well. Hence, in this work, we are reporting the results determined by the 224Q-SA-(9,7) wavefunctions for all the complexes.

TABLE S12: Comparison of the lowest spin-free, spin-orbit energy levels (in cm^{-1}) and zero-field splitting parameters (in cm^{-1}) of the experimentally reported $\text{Fe}_{\text{Cl}}^{\text{D}}$ (np.) complex in the intermediate spin state with CAS(9,7) and CAS(9,12) active space with 2 and 4 number of roots.

		2(Q)			4(Q)						
CAS		Spin-free states	Spin-orbit states	D	E	U_{eff}	Spin-free states	Spin-orbit states	D	E	U_{eff}
CAS (9,7)	304.4		84.7	-42.3	0.0	84.7	365.7	73.2	-36.6	0.47	73.2
	-		416.8				5065.6	467.0			
							5919.1	553.3			
CAS (9,12)	352.9		69.8	-34.9	0.0	69.8	397.7	61.0	-30.5	0.38	61.0
	-		444.2				5693.1	481.4			
							6578.9	553.3			

Dynamic Electron Correlation

In multiconfigurational complete-active-space based methods, the electronic correlation is evaluated in two steps. The first step is CASSCF, in which a suitable wavefunction is determined by careful choice of orbital in the active space. It takes care of the static electron correlation. To obtain reliable energies, additional dynamical correlation not recovered at the CASSCF level must be included. This can be done on top of a CASSCF reference wavefunction by using second-order perturbation theory approaches, such as complete active space second-order perturbation theory (CASPT2) or N-electron valence perturbation theory (NEVPT2). It should be pointed out that there exist alternative methods, such as equation-of-motion coupled-cluster-based approaches that can efficiently describe electronic excited states and recover both static and dynamic electron correlation [1]. However, in the context of this article, we are specifically employing the complete-active-space based approach. Therefore, to investigate the effect of dynamic electron correlation on the spin-state energetics, we subjected the 224Q-SA-(9,7) computed wavefunctions of both the planar and non-planar $\text{Fe}_{\text{Cl}}^{\text{P}}$ conformers to the multi-state (MS)- and extended multi-state (XMS)-CASPT2 calculations with OpenMolcas program [2, 3]. In all the MS- and XMS-CASPT2 calculations the standard definition of zero-order Hamiltonian ($\text{IPEA} = 0.25 \text{ a.u.}$) is used. To exclude the possible intruder states a vertical shift of 0.5 a.u. is applied. For the non-planar complex, the MS-CASPT2 computed $\Delta E_{Q_1-Q_0}$ is observed to vary between $587\text{-}617 \text{ cm}^{-1}$, upon the number of states considered for the calculation. On the other hand, the magnitude of $\Delta E_{Q_1-Q_0}$ varies between 670 to 981 cm^{-1} when computed with XMS-CASPT2 method, starting from the same reference CASSCF wavefunction. Similarly, for the planar complex, the MS-CASPT2 computed $\Delta E_{Q_1-Q_0}$ varies between 379 to 398 cm^{-1} , and the same with XMS-CASPT2 method is 445 to 533 cm^{-1} . The discrepancies between the MS-, and XMS-CASPT2 energy levels are not unusual [4]. Observing these deviations between the two CASPT2 approaches, we also performed NEVPT2 calculations starting from the same CASSCF wave function. However, the NEVPT2 computed energetics also appeared to differ significantly from those shown by the two CASPT2 methods (Table S13 in ESI). It is already established that the $\Delta E_{Q_1-Q_0}$ plays a significant role in determining the spin-orbit energy levels, hence the magnitudes of D and U_{eff} as well. Therefore, based on the inconsistencies shown, the second-order perturbation theory was excluded from determining the spin-state energetics and the magnetic anisotropy parameters with reasonable accuracy. Hence, in

TABLE S13: Comparison of MS-CASPT2, XMS-CASPT2 and NEVPT2, results with different number of roots for $\text{Fe}_{\text{Cl}}^{\text{P}}$ (pl.), $\text{Fe}_{\text{Cl}}^{\text{P}}$ (np.) complexes. NEVPT2 calculations did not converge when 80 quartets were considered.

$\text{Fe}_{\text{Cl}}^{\text{P}}$ (pl.)										$\text{Fe}_{\text{Cl}}^{\text{P}}$ (np.)											
Method	Spin-free states					Spin-orbit states					Spin-free states					Spin-orbit states					
	2(Q)	4(Q)	12(Q)	80(Q)	2(Q)	4(Q)	12(Q)	80(Q)	2(Q)	4(Q)	12(Q)	80(Q)	2(Q)	4(Q)	12(Q)	80(Q)	2(Q)	4(Q)	12(Q)	80(Q)	
MS-CASPT2	0.0	0.0	0.0	0.0	0.0	0.0	0.0	0.0	0.0	0.0	0.0	0.0	0.0	0.0	0.0	0.0	0.0	0.0	0.0	0.0	
	394.1	394.1	397.9	378.7	58.5	56.1	54.5	53.9	616.9	616.9	616.3	588.6	41.2	37.8	36.7	36.2	6615.8	6615.6	6672.5		
			7066.8	7071.1	7114.3												7733.9	7733.3	7783.3		
			7097.2	7085.9	7135.9																
XMS-CASPT2	0.0	0.0	0.0	0.0	0.0	0.0	0.0	0.0	0.0	0.0	0.0	0.0	0.0	0.0	0.0	0.0	0.0	0.0	0.0	0.0	
	465.9	476.5	533.1	444.5	51.7	48.5	42.8	47.5	670.1	758.8	981.2	688.6	38.3	31.2	22.8	31.3	7792.2	8140.2	8002.6		
			8230.0	8271.0	8315.6												8894.3	8872.6	9063.7		
NEVPT2	0.0	0.0	0.0		0.0	0.0	0.0		0.0	0.0	0.0	0.0	0.0	0.0	0.0	0.0	0.0	0.0	0.0	0.0	
	78.8	68.04	101.0		127.1	127.2	118.7		334.7	368.5	458.7		-	87.2	78.5	58.4					
			6257.6	7169.6													5711.0	6741.8			
			6448.1	7594.9													6870.8	7883.9			

this article, we report the spin-state energetics and the magnetic anisotropy parameters determined by the CASSCF energies.

-
- [1] P. Pokhilko, E. Epifanovsky, and A. I. Krylov, *J. Chem. Phys.* **151**, 034106 (2019).
 - [2] F. Aquilante, J. Autschbach, A. Baiardi, S. Battaglia, V. A. Borin, L. F. Chibotaru, I. Conti, L. De Vico, M. Delcey, I. Fdez. Galván, N. Ferré, L. Freitag, M. Garavelli, X. Gong, S. Knecht, E. D. Larsson, R. Lindh, M. Lundberg, P. Malmqvist, A. Nenov, J. Norell, M. Odelius, M. Olivucci, T. B. Pedersen, L. Pedraza-González, Q. M. Phung, K. Pierloot, M. Reiher, I. Schapiro, J. Segarra-Martí, F. Segatta, L. Seijo, S. Sen, D.-C. Sergentu, C. J. Stein, L. Ungur, M. Vacher, A. Valentini, and V. Veryazov, *J. Chem. Phys.* **152**, 214117 (2020).
 - [3] I. F. Galván, M. Vacher, A. Alavi, C. Angeli, F. Aquilante, J. Autschbach, J. J. Bao, S. I. Bokarev, N. A. Bogdanov, R. K. Carlson, L. F. Chibotaru, J. Creutzberg, N. Dattani, M. G. Delcey, S. S. Dong, A. Dreuw, L. Freitag, L. M. Frutos, L. Gagliardi, F. Gendron, A. Giussani, L. González, G. Grell, M. Guo, C. E. Hoyer, M. Johansson, S. Keller, S. Knecht, G. Kovačević, E. Källman, G. L. Manni, M. Lundberg, Y. Ma, S. Mai, J. P. Malhado, P. Å. Malmqvist, P. Marquetand, S. A. Mewes, J. Norell, M. Olivucci, M. Oppel, Q. M. Phung, K. Pierloot, F. Plasser, M. Reiher, A. M. Sand, I. Schapiro, P. Sharma, C. J. Stein, L. K. Sørensen, D. G. Truhlar, M. Ugandi, L. Ungur, A. Valentini, S. Vancoillie, V. Veryazov, O. Weser, T. A. Wesołowski, P.-O. Widmark, S. Wouters, A. Zech, J. P. Zobel, and R. Lindh, *J. Chem. Theory Comput.* **15**, 5925 (2019).
 - [4] M. Godsall and N. F. Chilton, *J. Phys. Chem. A* **126**, 6059 (2022).